Physics Letters B 811 (2020) 135901

Contents lists available at ScienceDirect

Physics Letters B

www.elsevier.com/locate/physletb

Hydrodynamization in systems with detailed transverse profiles

Aleksi Kurkela [a,b], Seyed Farid Taghavi [c], Urs Achim Wiedemann [a], Bin Wu [a]

[a] Theoretical Physics Department, CERN, CH-1211 Genève 23, Switzerland
[b] Faculty of Science and Technology, University of Stavanger, 4036 Stavanger, Norway
[c] Physik Department E62, Technische Universität München, James Franck Str. 1, 85748 Garching, Germany

ARTICLE INFO

Article history:
Received 16 August 2020
Received in revised form 20 October 2020
Accepted 22 October 2020
Available online 9 November 2020
Editor: W. Haxton

ABSTRACT

The observation of fluid-like behavior in nucleus-nucleus (AA), proton-nucleus (pA) and high-multiplicity proton-proton (pp) collisions motivates systematic studies of how different measurements approach their fluid-dynamic limit. We have developed numerical methods to solve the ultra-relativistic Boltzmann equation for systems of arbitrary size and transverse geometry. Here, we apply these techniques for the first time to the study of azimuthal flow coefficients v_n including non-linear mode-mode coupling and to an initial condition with realistic event-by-event fluctuations. We show how both linear and non-linear response coefficients extracted from v_n develop as a function of opacity from free streaming to perfect fluidity. We note in particular that away from the fluid-dynamic limit, the signal strength of linear and non-linear response coefficients does not reduce uniformly, but that their hierarchy and relative size shows characteristic differences.

1. Introduction

Hydrodynamization denotes the transition to hydrodynamics of systems that carry fluid- and non-fluid-dynamic degrees of freedom and that therefore do not need to behave fluid dynamically at all times and under all conditions. The observation of strong signs of collectivity in ultra-relativistic nucleus-nucleus (AA), proton-nucleus (pA) and proton-proton (pp) collisions [1–3] has motivated in recent years many studies of *hydrodynamization* in strongly- and weakly-coupled models of quark-gluon plasma [4–31]. Their ultimate aim is to provide a rigorous underpinning of the fluid-dynamic interpretation of collective flow in AA, pA and pp collisions, and to delineate the limitations of any such interpretation.

Most studies of hydrodynamization profit from simplified setups that do not reflect all phenomenological complications but that exhibit general features in great clarity. In particular, most studies of hydrodynamization to date assume exact Bjorken boost invariance, employ conformally symmetric collective dynamics and focus on dimensionally reduced $1+1$D systems [4–7,9–12,14–17,19] (for studies extending this framework, see [13,18,20–26,32]). Within this setting, one has reached in recent years a thorough understanding of the off-equilibrium evolution of simple observables in various models. For instance, the asymmetry p_T/p_L between longitudinal and transverse pressure and the higher longitudinal momentum moments of the stress-energy tensor are known to approach rapidly their universal attractor solution in kinetic theory [33,26,16]. The mathematical structures behind this behavior continue to be studied in the context of resurgence [9,10,27,28].

The lessons learnt from these $1+1$D systems are expected to carry over to the phenomenological reality in $3+1$D. For instance, the early-time dynamics of p_T/p_L in boost-invariant $3+1$D systems is known to be governed locally in the transverse plane by an effective $1+1$D evolution, and the $1+1$D universal attractor for p_T/p_L is therefore of relevance for the $3+1$D dynamics. However, very few observables of phenomenological relevance can be studied in $1+1$D systems, and some important questions have therefore received little attention so far in the debate of hydrodynamization. One of them is whether all bulk observables hydrodynamize under conditions comparable to those under which p_T/p_L hydrodynamizes, or whether some classes of observables require systems of longer lifetime, larger spatial extent and/or higher density to approach the values they attain under conditions of almost perfect fluidity. Of particular interest in this context are the conditions for hydrodynamization of the azimuthal momentum anisotropies v_n of soft multi-particle production, as these are amongst the most abundant and most precisely measured signatures of collective behavior in AA, pA and pp collisions. Here, we analyze their hydrodynamization in a boost invariant conformally symmetric $3+1$D kinetic transport theory, whose $1+1$D variants have been used repeatedly in studies of hydrodynamization.

E-mail address: urs.wiedemann@cern.ch (U.A. Wiedemann).

https://doi.org/10.1016/j.physletb.2020.135901

Up until this point, only the linear response coefficients have been studied in full kinetic theory because of the technical challenges related to solving Boltzmann equations for a distribution functions in complex geometries [34,25,26], though some results exist for perturbative solutions around free-streaming [35,34]. We have developed numerical techniques to solve such systems and we present here the first non-linear response coefficients, and we present the first solution to the Boltzmann equation for an initial condition with realistic event-by-event fluctuations.

2. Kinetic theory

We consider massless, boost-invariant kinetic theory in the isotropization-time approximation, and we restrict the discussion to the first momentum moments $F(\vec{x}_\perp, \Omega, \tau) = \int \frac{4\pi p^2 dp}{(2\pi)^3} p f$ of the distribution function f. Here, p is the modulus of the three-momentum, the velocity is $v_\mu \equiv p_\mu/p$ with $p_\mu\, p^\mu = 0$ and $v^0 = 1$, and Ω denotes the angular phase space of v_μ. F defines the energy momentum tensor $T^{\mu\nu} = \int d\Omega\, v^\mu v^\nu F$, as well as arbitrary higher v_μ-moments that lie beyond hydrodynamics. It satisfies the equations of motion [26]

$$\partial_\tau F + \vec{v}_\perp \cdot \partial_{\vec{x}_\perp} F - \frac{v_z}{\tau}(1-v_z^2)\partial_{v_z} F + \frac{4v_z^2}{\tau} F = -C[F] = -\gamma \varepsilon^{1/4}(x)[-v_\mu u^\mu](F - F_{\rm iso})\,, \tag{1}$$

where ε is the local energy density. Fluid-like and particle-like excitations are known to coexist in this kinetic transport and their properties can be calculated analytically. In particular, the coupling γ is related to the specific shear viscosity $\frac{\eta}{sT} = \frac{1}{5\gamma\varepsilon^{1/4}}$, and F relaxes locally on a time scale $\tau_R = \frac{1}{\gamma\varepsilon^{1/4}}$ to the isotropic distribution $F_{iso}(\tau, \vec{x}_\perp; \Omega) = \frac{\varepsilon(\tau,\vec{x}_\perp)}{(-u_\mu v^\mu)^4}$ whose functional form is fixed by symmetries and by the Landau matching condition, $u^\mu T_\mu{}^\nu = -\varepsilon u^\nu$.

As the dynamics (1) is scaleless, dimensionful characteristics of the collision system can enter only via the initial conditions, and they can affect results only in dimensionless combinations. For a system of transverse r.m.s. size R and energy density ε_0 at initial time τ_0, it follows that the opacity $\hat{\gamma} = \gamma R^{3/4}(\varepsilon_0\tau_0)^{1/4}$ is the unique model parameter. Eq. (1) interpolates between free-streaming in the limit of vanishing opacity $\hat{\gamma} \to 0$ and ideal fluid dynamics in the limit $\hat{\gamma} \to \infty$.

To initialize (1) with "realistic" initial conditions, we determine $F(\tau_0, \vec{x}_\perp; \phi, v_z)$ from the T_RENTo [36] parametrization of the initial transverse energy density. This is the current standard in phenomenological studies and it includes large event-by-event fluctuations. One T_RENTo event seeds many linear and non-linear response coefficients. Alternatively, to study individual linear and non-linear response coefficients, we seed an often used simple Gaussian ansatz (see, e.g., [37,34,26]) with one or very few small perturbations δ_n

$$F(\tau_0, \vec{x}_\perp; \phi, v_z) = 2\varepsilon_0\, \delta(v_z)\, \exp\left[-\frac{r^2}{R^2}\right] \times \left(1 + \sum_n \delta_n \left(\frac{r}{R}\right)^n \cos\left(n\theta - n\psi_n\right) \exp\left[-\frac{r^2}{2R^2}\right]\right). \tag{2}$$

The initial spatial azimuthal asymmetries are proportional to the real factors δ_n, and they are oriented along the azimuthal directions ψ_n. The exponential $\exp\left[-\frac{r^2}{2R^2}\right]$ multiplying the cos-term ensures that the distribution stays positive everywhere for sufficiently small δ_n's. As our numerical techniques apply to events with arbitrarily large fluctuations, we can check to what extent the lessons learnt from studying (2) carry over to "realistic" events.

For both classes of initial conditions, we quantify azimuthal anisotropies in terms of the complex-valued spatial eccentricities for $n > 1$,

$$\epsilon_n \equiv -\frac{\int d\theta\, r\, dr\, r^n \exp\left[in\theta\right]\, F(\tau_0, \vec{x}_\perp; \Omega)}{\int d\theta\, r\, dr\, r^n F(\tau_0, \vec{x}_\perp; \Omega)} \equiv |\epsilon_n|\, e^{i n \psi_n}\,. \tag{3}$$

Evolving with eq. (1) the initial conditions (2), we obtain the evolution of the energy-momentum tensor $T^{\mu\nu}$ and the transverse energy flow $dE_\perp$ at late times

$$\frac{dE_\perp}{d\eta_s d\phi} \equiv \int dp_\perp^2 \frac{p_\perp\, dN}{dp_\perp^2\, d\eta_s d\phi} = \frac{dE_\perp}{2\pi\, d\eta_s}\left(1 + 2\sum_{n=1}^{\infty} v_n \cos\left(n\,\phi - n\,\phi_n\right)\right). \tag{4}$$

This determines the energy flow coefficients $V_n = v_n\, e^{i n \phi_n}$, where ϕ_n is the azimuthal orientation of the energy flow. In contrast to flow coefficients extracted from particle distributions dN, our study focuses on energy-flow coefficients which are not affected by hadronization since hadronization conserves energy and momentum.

The viscous fluid-dynamic limit of eq. (1) is restricted to the evolution of seven fluid-dynamic fields which may be identified with those seven components of $T^{\mu\nu}(\tau, \vec{x}_\perp) = \int d\Omega\, v^\mu v^\nu F$ that do not vanish under boost-invariance. We are interested in the apparently simple kinetic theory (1) for $F(\tau, \vec{x}_\perp; \phi, v_z)$ away from the fluid dynamics limit since it provides an explicit realization of fluid fields coupled to a tower of arbitrarily many non-fluid-dynamic excitations (that may be parametrized by the higher v^μ-moments of F). However, going beyond the fluid-dynamic limit has a price: F depends on two additional dimensions ϕ and v_z in momentum space. Discretizing ϕ in twenty points and discretizing the v_z-dependence in 50 points implies a 1000-fold increase of the numerical complexity compared to viscous fluid dynamics. The numerical method for solving this evolution equation (1) has been described in [26], but there it was applied only to the linear response of flow coefficients for infinitesimally small ϵ_n when the coupling between different harmonics can be neglected and the numerics simplifies. Here, we overcome this remaining limitations and we study the kinetic theory for arbitrary eccentricities, arbitrary opacities, and arbitrary coupled non-linear responses.

3. Results for mode-by-mode kinetic theory

The coefficients v_n are known to arise from the dynamical response to spatial eccentricities ϵ_n in the initial nuclear overlap. The numerically largest responses are linear ($v_n \propto w_{n;n}\epsilon_n$) [38], but sizable quadratic ($\propto w_{n;n_1,n_2}\epsilon_{n_1}\epsilon_{n_2}$) and cubic corrections have been quantified [39,40] and these can dominate higher harmonics ($n \geq 4$). For linear responses to spatial eccentricities, there is an intrinsic ambiguity between the initial geometry that specifies the values ϵ_n, and the collective dynamics that builds up v_n from these ϵ_n. Non-linear response coefficients are of particular interest, since they help to disentangle this ambiguity.

As a first example, we consider initial conditions (2) in which a single mode δ_2 is excited ($\delta_n = 0$ for $n \neq 2$). In the course of the evolution, the non-linear mode-mode coupling of this initial second harmonic with itself excites 4th, 6th, 8th, ... harmonics, but also the 0th harmonic. In turn, these higher harmonics affect the non-linear response of v_2. For this reason, numerical studies of the non-linear response to v_2 require sufficiently fine discretization in

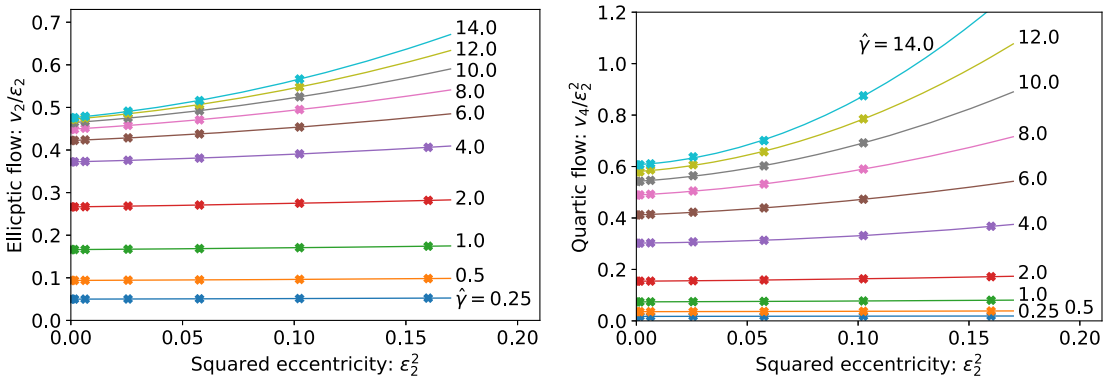

Fig. 1. Elliptic v_2 (left panel) and quartic v_4 (right panel) energy flow coefficients, divided by the leading power ϵ_2 and ϵ_2^2 of the perturbative expansion (5), respectively. Results of the kinetic theory (1), with initial conditions (2) seeded by a single non-vanishing elliptic eccentricity are displayed for different values of the opacity $\hat{\gamma}$ and as a function of the squared eccentricity $(\epsilon_2 \epsilon_2^*)$.

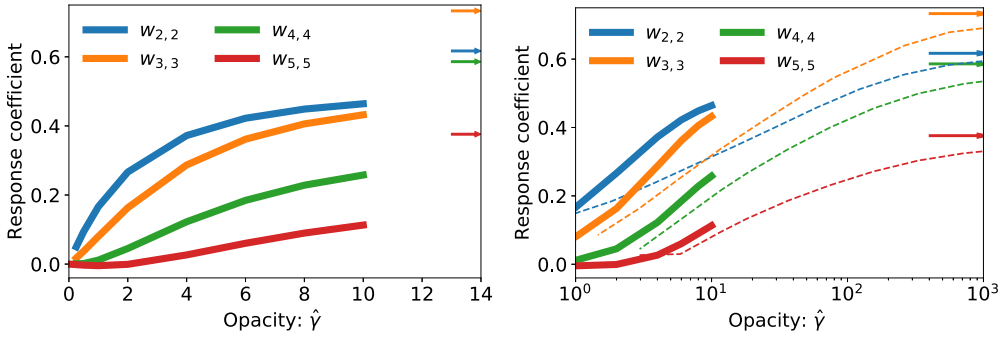

Fig. 2. Left panel: the linear response coefficients $w_{n,n} = \lim_{\epsilon_n \to 0} \frac{v_n}{\epsilon_n}$ calculated for the kinetic theory (1), (2) as a function of opacity $\hat{\gamma}$ (thick lines). Arrows at the right indicate values in the ideal-fluid limit corresponding to $\hat{\gamma} \to \infty$. Right panel: Same as in left panel but in semi-logarithmic presentation and overlaid with results from viscous fluid dynamics (thin dashed lines).

the momentum angle ϕ to follow numerically also the higher excited harmonics. The numerical results shown here were obtained for a ϕ-range discretized with 40 points, and their numerical stability was checked with finer discretizations. Our first main result is to observe that the non-linearities are more important for large opacity, as the lines in Fig. 1 develop larger slopes and curvatures. While the numerical results for v_2 and v_4 in Fig. 1 do not involve a perturbative expansion in ϵ_n or $\hat{\gamma}$, symmetry arguments imply that they must agree for sufficiently small ϵ_2 with the perturbative series

$$V_2 = w_{2,2}\epsilon_2 + w_{2,222}\left(\epsilon_2 \epsilon_2^*\right)\epsilon_2 + O(|\epsilon_2|^5)\,,$$
$$V_4 = w_{4,22}\epsilon_2^2 + O(|\epsilon_2|^4)\,. \tag{5}$$

According to eq. (5), the response coefficient $w_{2,2}(\hat{\gamma})$ at a given opacity $\hat{\gamma}$ is the intercept $\lim_{\epsilon_2^2 \to 0} \frac{v_2}{\epsilon_2}(\epsilon_2^2)$ of the corresponding curve in Fig. 1 with the ordinate. The non-linear response coefficient $w_{2,222}(\hat{\gamma})$ is the slope of the same curves in Fig. 1 at $\epsilon_2^2 = 0$. Similarly, one finds the non-linear response $w_{4,22}(\hat{\gamma}) = \lim_{\epsilon_2^2 \to 0} \frac{v_4}{\epsilon_2^2}(\epsilon_2^2)$. For notational simplicity, we do not denote explicitly the phases of the eccentricities in the following as these can be inferred easily from symmetry arguments. Fig. 2 shows the $\hat{\gamma}$-dependence of the linear response coefficient extracted from Fig. 1 in this way.

In close analogy, we determine other linear and non-linear response coefficients numerically by seeding the initial conditions with suitable choices of eccentricities. To determine the linear response coefficients $w_{n,n}(\hat{\gamma})$, $n \leq 5$, shown in Fig. 2, we run simulations seeded with a single n-th harmonic for different values of ϵ_n, and we extrapolate to $\lim_{\epsilon_n^2 \to 0} \frac{v_n}{\epsilon_n}(\epsilon_n^2)$, see Fig. 2. For the non-linear response coefficients $w_{n,m_1 m_2}$ ($n = m_1 + m_2$ or $= |m_1 - m_2|$), displayed in Fig. 3, we pick initial data with non-vanishing ϵ_{m_1}, ϵ_{m_2} and all other eccentricities vanishing. Extrapolating from simulations for different initial values of ϵ_{m_1}, ϵ_{m_2}, we determine $w_{n,m_1 m_2} = \lim_{\epsilon_{m_1}, \epsilon_{m_2} \to 0} \frac{v_n}{\epsilon_{m_1} \epsilon_{m_2}}$.

We ask next how the linear and non-linear response coefficients in Figs. 2 and 3 hydrodynamize, *i.e.*, how they approach their fluid-dynamic limit with increasing opacity $\hat{\gamma}$. To this end, we relate the opacity that characterizes kinetic transport to quantities accessible in viscous fluid dynamics. The definition $\hat{\gamma} = \gamma\, R^{3/4}\, (\varepsilon_0\, \tau_0)^{1/4}$ assumes that the early-time evolution is given by free-streaming which is not the case for viscous fluid dynamics. We therefore have to work with an equivalent definition that can be expressed in terms of quantities measured at a time at which the flow builds up and fluid dynamics may be operational. To this end, we write

$$\hat{\gamma} = \gamma\, R \left(\frac{\varepsilon_R}{f_{0\to R}(\hat{\gamma})} \right)^{1/4}\,, \tag{6}$$

where, for the Gaussian background in the initial condition (2), ε_0 and ε_R denote central ($r = 0$) energy densities at times τ_0 and R, respectively. The function $f_{0\to R}(\hat{\gamma}) = \frac{\varepsilon_R R}{\varepsilon_0 \tau_0}$ is defined as the ratio of the energy per unit rapidity at time $\tau = R$ to the energy which the system would have if it were free-streaming [26]. We calculate $f_{0\to R}(\hat{\gamma})$ from kinetic theory for $\hat{\gamma} \leq 10$, and we match for larger $\hat{\gamma}$ to the known asymptotic large-$\hat{\gamma}$ behavior $f_{0\to R} \sim \hat{\gamma}^{-4/9}$.

With $f_{0\to R}(\hat{\gamma})$ known, we relate viscous fluid-dynamic calculations to $\hat{\gamma}$ by specifying ε_R and η/s from fluid dynamics and solving eq. (6) for $\hat{\gamma}$. In particular, we use the kinetic relation between the interaction strength γ and the shear viscosity $\frac{\eta}{sT} = \frac{1}{5\gamma\varepsilon^{1/4}}$. We

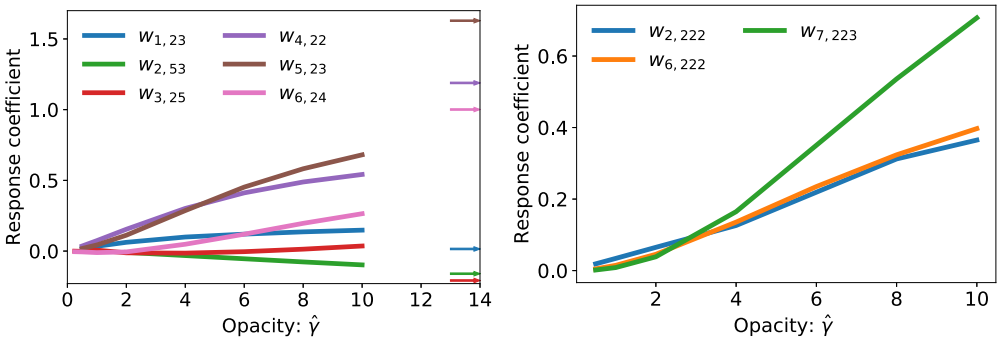

Fig. 3. Left panel: Quadratic response coefficients calculated from the kinetic theory (1), (2) (thick lines) and their ideal-fluid limits corresponding to $\hat{\gamma} \to \infty$ (arrows). Right panel: Cubic response coefficients from the same kinetic theory.

then initialize at some initial time $\tau_0 < R$ the components of $T^{\mu\nu}$ from the same initial conditions (2) as the kinetic theory and we evolve them with viscous fluid dynamics for varying $\frac{\eta}{s}$ and ε_0. This allows us to determine ε_R and $\hat{\gamma}$, and to extract from the transverse energy flow (4) at late times the energy-flow coefficients v_n. In general, these results depend on τ_0. That the $\tau_0 \to 0$-limit of $v_n(\hat{\gamma})$ exists is a direct consequence of the fact that viscous fluid dynamics, like kinetic theory, has a universal attractor solution at arbitrarily early times [12]. While the attractor of kinetic theory keeps $\varepsilon\tau$ fixed leading to the scaling of $\hat{\gamma} = \gamma\, R^{3/4}\, (\varepsilon_0\, \tau_0)^{1/4}$, the attractor of the viscous (Israel-Stewart) hydrodynamics considered here keeps $\varepsilon\tau^{\frac{4}{15}\left(\sqrt{5}-5\right)}$ constant [13]. Therefore taking the $\tau_0 \to 0$ limit while keeping $\hat{\gamma}$ as defined in eq. (6) fixed corresponds to scaling initial energy densities by $\varepsilon(\tau_0) \propto \tau_0^{-\frac{4}{15}\left(\sqrt{5}-5\right)}$. While this non-standard procedure differs from the common phenomenological practice, it allows for a particularly clean comparison between kinetic theory and fluid dynamics by eliminating the unphysical model parameter τ_0. The difference between the kinetic theory and fluid-dynamic results obtained this way do not inform us on the validity or the breakdown of the current phenomenological practice. Instead it emphasizes the importance of the early-time attractor (which differs between kinetic theory and the fluid dynamics) for the physical observables measured in experiments and it informs us about the extent to which the entire signal v_n is or is not build up by the degrees of freedom encoded in viscous fluid dynamics. For linear response coefficients, this comparison is shown in the right panel of Fig. 2.

Technically, we evolve the viscous fluid-dynamic equations as described in Ref. [41,42] by splitting all fluid dynamic fields into an azimuthally symmetric background and an azimuthally anisotropic perturbation and solving for them to first order in initial eccentricities. In the same way, we set up a control calculation for the much simpler ideal fluid-dynamic equations to obtain an independent determination of linear response coefficients in the limit $\hat{\gamma} \to \infty$ (arrows in Fig. 2). Results for $w_{2,2}$ and $w_{3,3}$ differ somewhat from those reported in [26] since the initial conditions are different. (Calculations in [26] are initialized at $\tau_0 = 0.1$, while here we take the $\tau_0 \to 0$-limit as described above. Also, the parametrization of the radial profile used in Ref. [26] differs from that of eq. (2).)

As expected from general reasoning, the viscous fluid-dynamic results for $\frac{v_n(\hat{\gamma})}{\epsilon_n}$ in the limit $\tau_0 \to 0$ asymptote for $\hat{\gamma} \to \infty$ to the ideal fluid-dynamic results in the same $\tau_0 \to 0$ limit, see Fig. 2. Remarkably, the hierarchy between the elliptic and triangular linear response coefficient gets inverted as a function of $\hat{\gamma}$: kinetic theory at low $\hat{\gamma}$ shows $w_{2,2} > w_{3,3}$ while ideal fluid dynamics shows $w_{2,2} < w_{3,3}$. Viscous fluid dynamics accounts for this inversion qualitatively: for very small specific shear viscosity $\frac{\eta}{s}$, *i.e.*, very large opacity $\hat{\gamma}$, it is consistent with ideal fluid dynamics, but the hierarchy changes as a function of opacity, see right panel of Fig. 2. Also the results from kinetic theory hint at such an inversion, as the slope of $w_{3,3}(\hat{\gamma} = 10)$ is larger than the slope of $w_{2,2}(\hat{\gamma} = 10)$.

As seen from Fig. 2, viscous fluid dynamics reproduces the main qualitative trends of kinetic theory (hierarchy of response coefficients) at $\hat{\gamma} \sim O(10)$, but significant quantitative differences persist. On general grounds, we expect that kinetic theory matches quantitatively to viscous fluid dynamics at sufficiently large $\hat{\gamma}$ when the fluid dynamic gradient expansion becomes quantitatively reliable. All data shown here are consistent with this expectation. It would clearly be interesting to extend the numerical calculations in kinetic theory to larger $\hat{\gamma}$ and to determine the $\hat{\gamma}$-scale at which a seamless matching to viscous fluid dynamics is found. However, with increasing $\hat{\gamma}$, the numerical evaluation becomes more expensive, and within the scope of the present letter, we were not able to push to higher $\hat{\gamma}$.

We have extended this analysis to a set of quadratic and cubic response coefficients, see Fig. 3. To make some statements about their hydrodynamization we determine the quadratic response coefficients in the limit $\hat{\gamma} \to \infty$ by solving ideal fluid dynamics to second order in eccentricities (arrows in Fig. 3). Within the range $\hat{\gamma} < 10$, several quadratic response coefficients are seen to cross, and at $\hat{\gamma} = 10$, the hierarchy of the numerically large response coefficients ($w_{5,23} > w_{4,22} > w_{6,24}$) found in kinetic theory is consistent with that of ideal fluid dynamics. In the range $\hat{\gamma} > 10$, the numerically smaller response coefficients $w_{3,25}$ and $w_{2,53}$ need to cross. These observations give further support to the conclusions reached from Fig. 2.

In a remarkable note [35], it was observed already that in the dilute limit of kinetic theory far from equilibrium, linear and quadratic response coefficients grow linearly in the average number of rescatterings $\bar{N}_{\text{resc.}}$ while cubic ones have a quadratic dependence. In Ref. [35], this scaling was established for elastic two-to-two collision kernels. The line of arguments of Ref. [35] does not apply to the collision kernel (1). However, a perturbative expansion of (1) in $\hat{\gamma}$ can be viewed as an expansion in the average number of scattering centers [34], and it is therefore natural to test whether our results show this same scaling, too. For linear and quadratic coefficients, we know already from the perturbative analysis in [34] that they do. For cubic response coefficients, however, we observe small violations of the scaling. In the neighborhood of $\hat{\gamma} = 0$, the cubic coefficients in the right panel of Fig. 3 show a small linear component, though the quadratic one can be dominant.

4. Evolving initial conditions with realistic event-by-event fluctuations in kinetic theory

We now apply our newly developed numerical machinery to the first exploratory study of a realistic initial condition that would be one single event in an event sample of an event-by-

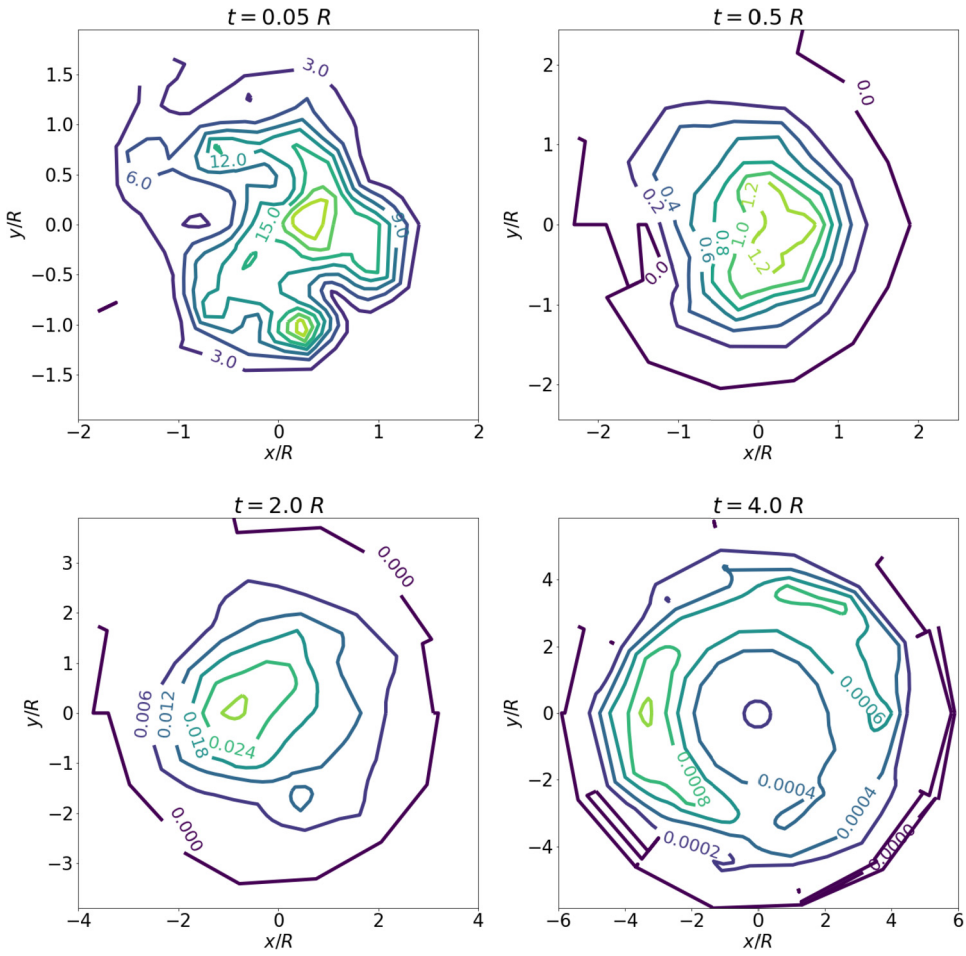

Fig. 4. Energy density in the transverse plane initialized with the T$_\mathrm{R}$ENTo model at $\tau_0/R = 0.05$ and evolved for $\hat{\gamma} = 2$ with the kinetic theory up to times $\tau/R = 0.05$, 0.5, 2.0 and 4.0, respectively.

event analysis. The initial condition is a typical T$_\mathrm{R}$ENTo event [36] in the $5-10\%$ centrality class smoothened such that only initial ϵ_n's for $n \leq 7$ are kept. We have checked that the finesse of our discretization allows for the stable propagation of such events. A typical time evolution is shown in Fig. 4 with $\hat{\gamma} = 2$. It illustrates that the Boltzmann equation can be solved non-perturbatively for distribution functions representing realistic initial conditions.

The radial profile of the T$_\mathrm{R}$ENTo event studied here differs from (2) and this can affect the value of linear and non-linear response coefficients. To quantify the difference, we compare the $w_{2,2}$ extracted for these two profiles and find the following numbers $w_{2,2}^{(\mathrm{T_R ENTo})} = \frac{v_2}{\epsilon_2}|_{\mathrm{T_R ENTo}, n=2} = 0.156$, 0.239, 0.288 and 0.319, compared to $w_{2,2}(\hat{\gamma}) = 0.166$, 0.266, 0.327 and 0.372 taken from Fig. 2 for $\hat{\gamma} = 1, 2, 3, 4$. Technically, $w_{2,2}^{\mathrm{T_R ENTo}}$ is not a linear response coefficient, since it was extracted at finite eccentricity, but Fig. 1 informs us that the numerical contribution arising from finite eccentricity is negligible for small opacity. We checked this for the T$_\mathrm{R}$ENTo profile as well (data not shown). We observe that the dependence on the radial profile in the linear response coefficients ranges from 5% to 15% in this $\hat{\gamma}$-range. The analogous study of $w_{3,3}$ shows a 2% to 10% difference in the same $\hat{\gamma}$-range. Therefore, the open circles in Fig. 5 are accounted for within 2% - 15% accuracy by the linear response coefficients calculated from the simplified profile (2). The remaining difference between open circles and full results in Fig. 5 result from mode-mode couplings of different harmonics. We see that while the linear response covers the ballpark of the results, non-linearities have to be included to go reliably beyond 20%-30% accuracy. The non-linearities generated by the lowest harmonics $n \leq 3$ account for half of all the non-linearities.

This paper is motivated by the wealth of studies of hydrodynamization and thermalization in simplified settings. We have developed the necessary machinery for overcoming many of these simplifications and to facilitate studies of hydrodynamization in complex realistic geometries, and to thus push the study of hydrodynamization from *in vitro* to *in vivo*. The ability to solve the Boltzmann equation for ultra-relativistic systems with realistic initial geometries and including all non-linear mode-mode couplings provides insight into how the characteristic features of fluid dynamics emerge gradually with increasing interaction strength. Away from the fluid dynamic limit, signals of collectivity are not simply reduced uniformly in size, but their relative strength varies characteristically with opacity, the hierarchy of the dominant linear response coefficients is inverted and so is the hierarchy of several non-linear ones. This may provide novel possibilities for characterizing to what extent systems of different size do or do not hydrodynamize. In the long run, we hope that the technical advances documented here can be developed further to study the evolution of event samples, and to study Boltzmann equations with other phenomenologically relevant complications, such as the propagation of massive degrees of freedom, a more realistic equation of state, or different collision kernels.

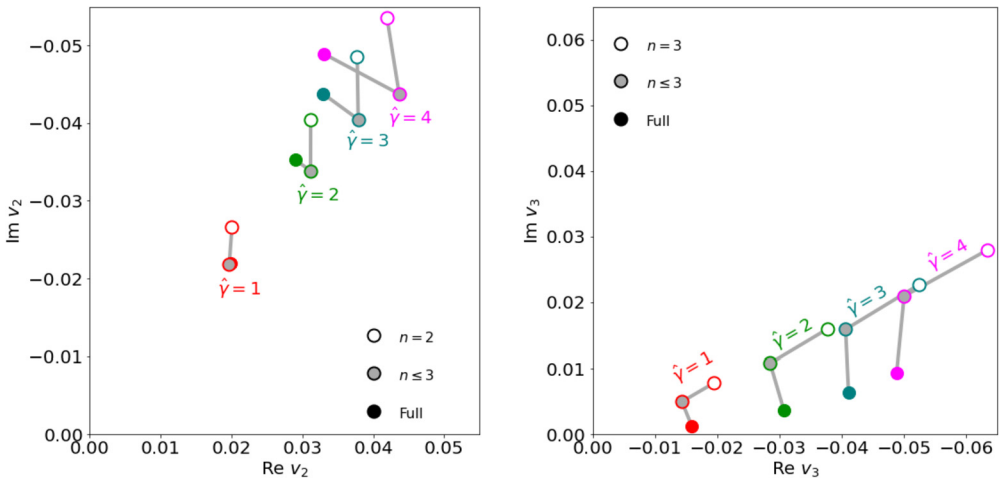

Fig. 5. The value of the elliptic and triangular flow coefficients evaluated for the same T$_R$ENTo event and for different opacities $\hat{\gamma}$. Results for the *full* event including harmonics $n \leq 7$ are compared to simplified events in which only specific harmonics are kept. (For $\hat{\gamma} = 1$, the circles for $n \leq 3$ and *full* event overlap in the left plot.)

Declaration of competing interest

The authors declare that they have no known competing financial interests or personal relationships that could have appeared to influence the work reported in this paper.

Acknowledgements

One of us (SFT) has received funding from the European Research Council (ERC) under the European Unions Horizon 2020 research and innovation programme (grant agreement No. 759257).

References

[1] B.B. Abelev, et al., ALICE Collaboration, Phys. Rev. C 90 (5) (2014) 054901, arXiv:1406.2474 [nucl-ex].
[2] A.M. Sirunyan, et al., CMS Collaboration, Phys. Rev. Lett. 120 (9) (2018) 092301, https://doi.org/10.1103/PhysRevLett.120.092301, arXiv:1709.09189 [nucl-ex].
[3] M. Aaboud, et al., ATLAS Collaboration, Eur. Phys. J. C 77 (6) (2017) 428, https://doi.org/10.1140/epjc/s10052-017-4988-1, arXiv:1705.04176 [hep-ex].
[4] P.M. Chesler, L.G. Yaffe, Phys. Rev. Lett. 102 (2009) 211601, https://doi.org/10.1103/PhysRevLett.102.211601, arXiv:0812.2053 [hep-th].
[5] M.P. Heller, R.A. Janik, P. Witaszczyk, Phys. Rev. Lett. 108 (2012) 201602, https://doi.org/10.1103/PhysRevLett.108.201602, arXiv:1103.3452 [hep-th].
[6] A. Kurkela, Y. Zhu, Phys. Rev. Lett. 115 (18) (2015) 182301, https://doi.org/10.1103/PhysRevLett.115.182301, arXiv:1506.06647 [hep-ph].
[7] L. Keegan, A. Kurkela, P. Romatschke, W. van der Schee, Y. Zhu, J. High Energy Phys. 1604 (2016) 031, https://doi.org/10.1007/JHEP04(2016)031, arXiv:1512.05347 [hep-th].
[8] J. Berges, M.P. Heller, A. Mazeliauskas, R. Venugopalan, arXiv:2005.12299 [hep-th].
[9] M.P. Heller, M. Spalinski, Phys. Rev. Lett. 115 (7) (2015) 072501, https://doi.org/10.1103/PhysRevLett.115.072501, arXiv:1503.07514 [hep-th].
[10] M.P. Heller, A. Kurkela, M. Spaliński, V. Svensson, Phys. Rev. D 97 (9) (2018) 091503, https://doi.org/10.1103/PhysRevD.97.091503, arXiv:1609.04803 [nucl-th].
[11] M.P. Heller, R.A. Janik, P. Witaszczyk, Phys. Rev. Lett. 110 (21) (2013) 211602, https://doi.org/10.1103/PhysRevLett.110.211602, arXiv:1302.0697 [hep-th].
[12] P. Romatschke, Phys. Rev. Lett. 120 (1) (2018) 012301, https://doi.org/10.1103/PhysRevLett.120.012301, arXiv:1704.08699 [hep-th].
[13] A. Kurkela, W. van der Schee, U.A. Wiedemann, B. Wu, Phys. Rev. Lett. 124 (10) (2020) 102301, https://doi.org/10.1103/PhysRevLett.124.102301, arXiv:1907.08101 [hep-ph].
[14] M. Strickland, J. Noronha, G. Denicol, Phys. Rev. D 97 (3) (2018) 036020, https://doi.org/10.1103/PhysRevD.97.036020, arXiv:1709.06644 [nucl-th].
[15] J.P. Blaizot, L. Yan, Phys. Lett. B 780 (2018) 283, https://doi.org/10.1016/j.physletb.2018.02.058, arXiv:1712.03856 [nucl-th].
[16] D. Almaalol, A. Kurkela, M. Strickland, arXiv:2004.05195 [hep-ph].
[17] M. Spaliński, Phys. Lett. B 784 (2018) 21, https://doi.org/10.1016/j.physletb.2018.07.003, arXiv:1805.11689 [hep-th].
[18] A. Behtash, S. Kamata, M. Martinez, H. Shi, Phys. Rev. D 99 (11) (2019) 116012, https://doi.org/10.1103/PhysRevD.99.116012, arXiv:1901.08632 [hep-th].
[19] M. Strickland, https://doi.org/10.5506/APhysPolB.50.1243, arXiv:1904.00413 [hep-ph].
[20] P.M. Chesler, L.G. Yaffe, J. High Energy Phys. 10 (2015) 070, https://doi.org/10.1007/JHEP10(2015)070, arXiv:1501.04644 [hep-th].
[21] G.S. Denicol, J. Noronha, Phys. Rev. D 99 (11) (2019) 116004, https://doi.org/10.1103/PhysRevD.99.116004, arXiv:1804.04771 [nucl-th].
[22] H. Bantilan, P. Figueras, D. Mateos, Phys. Rev. Lett. 124 (19) (2020) 191601, https://doi.org/10.1103/PhysRevLett.124.191601, arXiv:2001.05476 [hep-th].
[23] M. Attems, J. Casalderrey-Solana, D. Mateos, D. Santos-Oliván, C.F. Sopuerta, M. Triana, M. Zilhão, J. High Energy Phys. 06 (2017) 154, https://doi.org/10.1007/JHEP06(2017)154, arXiv:1703.09681 [hep-th].
[24] M. Attems, Y. Bea, J. Casalderrey-Solana, D. Mateos, M. Triana, M. Zilhão, Phys. Rev. Lett. 121 (26) (2018) 261601, https://doi.org/10.1103/PhysRevLett.121.261601, arXiv:1807.05175 [hep-th].
[25] A. Kurkela, U.A. Wiedemann, B. Wu, Eur. Phys. J. C 79 (9) (2019) 759, https://doi.org/10.1140/epjc/s10052-019-7262-x, arXiv:1805.04081 [hep-ph].
[26] A. Kurkela, U.A. Wiedemann, B. Wu, Eur. Phys. J. C 79 (11) (2019) 965, https://doi.org/10.1140/epjc/s10052-019-7428-6, arXiv:1905.05139 [hep-ph].
[27] M.P. Heller, V. Svensson, Phys. Rev. D 98 (5) (2018) 054016, https://doi.org/10.1103/PhysRevD.98.054016, arXiv:1802.08225 [nucl-th].
[28] G. Basar, G.V. Dunne, Phys. Rev. D 92 (12) (2015) 125011, https://doi.org/10.1103/PhysRevD.92.125011, arXiv:1509.05046 [hep-th].
[29] M. Spaliński, Phys. Lett. B 776 (2018) 468, https://doi.org/10.1016/j.physletb.2017.11.059, arXiv:1708.01921 [hep-th].
[30] A. Behtash, C.N. Cruz-Camacho, M. Martinez, Phys. Rev. D 97 (4) (2018) 044041, https://doi.org/10.1103/PhysRevD.97.044041, arXiv:1711.01745 [hep-th].
[31] J. Brewer, L. Yan, Y. Yin, arXiv:1910.00021 [nucl-th].
[32] L. Keegan, A. Kurkela, A. Mazeliauskas, D. Teaney, J. High Energy Phys. 08 (2016) 171, https://doi.org/10.1007/JHEP08(2016)171, arXiv:1605.04287 [hep-ph].
[33] M. Strickland, J. High Energy Phys. 12 (2018) 128, https://doi.org/10.1007/JHEP12(2018)128, arXiv:1809.01200 [nucl-th].
[34] A. Kurkela, U.A. Wiedemann, B. Wu, Phys. Lett. B 783 (2018) 274–279, https://doi.org/10.1016/j.physletb.2018.06.064, arXiv:1803.02072 [hep-ph].
[35] N. Borghini, S. Feld, N. Kersting, Eur. Phys. J. C 78 (10) (2018) 832, https://doi.org/10.1140/epjc/s10052-018-6313-z, arXiv:1804.05729 [nucl-th].
[36] J.S. Moreland, J.E. Bernhard, S.A. Bass, Phys. Rev. C 92 (1) (2015) 011901, https://doi.org/10.1103/PhysRevC.92.011901, arXiv:1412.4708 [nucl-th].
[37] W. Broniowski, M. Chojnacki, W. Florkowski, A. Kisiel, Phys. Rev. Lett. 101 (2008) 022301, https://doi.org/10.1103/PhysRevLett.101.022301, arXiv:0801.4361 [nucl-th].
[38] K. Aamodt, et al., ALICE, Phys. Rev. Lett. 107 (2011) 032301, https://doi.org/10.1103/PhysRevLett.107.032301, arXiv:1105.3865 [nucl-ex].
[39] S. Acharya, et al., ALICE Collaboration, Phys. Lett. B 773 (2017) 68, https://doi.org/10.1016/j.physletb.2017.07.060, arXiv:1705.04377 [nucl-ex].
[40] D. Teaney, L. Yan, Phys. Rev. C 86 (2012) 044908, https://doi.org/10.1103/PhysRevC.86.044908, arXiv:1206.1905 [nucl-th].
[41] S. Floerchinger, U.A. Wiedemann, Phys. Lett. B 728 (2014) 407–411, https://doi.org/10.1016/j.physletb.2013.12.025, arXiv:1307.3453 [hep-ph].
[42] S. Floerchinger, U.A. Wiedemann, A. Beraudo, L. Del Zanna, G. Inghirami, V. Rolando, Phys. Lett. B 735 (2014) 305, https://doi.org/10.1016/j.physletb.2014.06.049, arXiv:1312.5482 [hep-ph].